Downloaded from orbit.dtu.dk on: Apr 19, 2024

DTU Library

# Time-resolved infrared photoluminescence spectroscopy using parametric three-wave mixing with angle-tuned phase matching

**Roesgaard, Søren; Meng, Lichun; Tidemand-Lichtenberg, Peter; Dam, Jeppe Seidelin; Rodrigo, Peter John; Pedersen, Christian; Julsgaard, Brian**

*Published in:*
Optics Letters

*Link to article, DOI:*
10.1364/OL.43.003001

*Publication date:*
2018

*Document Version*
Peer reviewed version

Link back to DTU Orbit

*Citation (APA):*
Roesgaard, S., Meng, L., Tidemand-Lichtenberg, P., Dam, J. S., Rodrigo, P. J., Pedersen, C., & Julsgaard, B. (2018). Time-resolved infrared photoluminescence spectroscopy using parametric three-wave mixing with angle-tuned phase matching. *Optics Letters*, *43*(12), 3001-3004. https://doi.org/10.1364/OL.43.003001

**General rights**
Copyright and moral rights for the publications made accessible in the public portal are retained by the authors and/or other copyright owners and it is a condition of accessing publications that users recognise and abide by the legal requirements associated with these rights.

- Users may download and print one copy of any publication from the public portal for the purpose of private study or research.
- You may not further distribute the material or use it for any profit-making activity or commercial gain
- You may freely distribute the URL identifying the publication in the public portal

If you believe that this document breaches copyright please contact us providing details, and we will remove access to the work immediately and investigate your claim.

# Time-resolved infra-red photoluminescence spectroscopy using parametric three-wave mixing with angle-tuned phase matching

SØREN ROESGAARD[1], LICHUN MENG[2], PETER TIDEMAND-LICHTENBERG[2], JEPPE SEIDELIN DAM[2], PETER JOHN RODRIGO[2], CHRISTIAN PEDERSEN[2], AND BRIAN JULSGAARD[1,3,*]

[1] *Interdisciplinary Nanoscience Center (iNano), Aarhus University, Gustav Wieds Vej 14, DK-8000 Aarhus C, Denmark.*
[2] *DTU Fotonik, Technical University of Denmark, Frederiksborgvej 399, DK-4000 Roskilde, Denmark.*
[3] *Department of Physics and Astronomy, Aarhus University, Ny Munkegade 120, DK-8000 Aarhus C, Denmark.*
[*] *Corresponding author: brianj@phys.au.dk*

**A setup for time-resolved photoluminescence spectroscopy, based on parametric three-wave mixing in a periodically poled lithium niobate crystal, is characterized. Special attention is given to adjusting the phase matching condition by angle tuning of the luminescent light relative to a strong, continuous-wave laser beam within the crystal. The detection system is capable of operating at room temperature and in a wavelength range from 1.55 μm to 2.20 μm. Its sensitivity is compared to a commercial photo multiplier, and its capability of nano-second time resolution is demonstrated.**

***OCIS codes:*** (300.6340) Infrared spectroscopy; (040.3060) Infrared detectors; (190.7220) Non-linear optics, upconversion; (300.6500) Time-resolved spectroscopy.

Time-resolved fluorescence spectroscopy is a powerful tool in various experimental sciences, since it is capable of distinguishing different processes based on both characteristic energies and time scales [1]. Experiments are typically carried out by pulsed laser excitation of the material under study, followed by a spectral selection in a monochromator and detection of the emitted light. Various time-resolving detectors are currently available, including photo-multiplier tubes (PMTs), avalanche photo diodes (APDs), and streak cameras, with timing resolutions in the sub-ns regime for PMTs and APDs and into the sub-ps regime for streak cameras. Such detectors are typically based on InP/InGaAs photo cathodes in commercial products and able to detect light with a wavelength up to 1.7 μm. Improved timing resolution can be obtained by optical gating, e.g. by parametric three-wave mixing of the emitted light in a non-linear $\chi^{(2)}$ material with femto-second laser pulses [2]. Such non-linear detection schemes also present a promising alternative for infrared (IR) detection in general. By mixing with a high-intensity laser field, the IR signal is upconverted (UC) to the visible or near-IR band where detectors with better performance are available. In comparison to conventional semiconductor-based IR detectors (InGaAs, HgCdTe , InAs, and InSb), an upconversion detector (UCD) shows higher detectivity at room temperature operation and its potential has already been demonstrated in applications such as hyperspectral imaging [3], gas analysis [4], and single-photon detection [5]. Recently, other IR detector technologies have emerged such as superconducting nanowire single-photon detectors [6] and the HgCdTe e-APD [7]. They show high quantum efficiency and low background noise, but operate at cryogenic temperature, and their detection bandwidth is limited by their specific scheme. On the contrary, an UCD operates at room temperature, which allows for a more compact and portable design. Moreover, the UCD can achieve high-bandwidth detection by simply choosing a high-bandwidth detector that works in the UC signal spectral range (typically a Si-based detector). The above-mentioned advantages of UCDs make them good candidate systems for time-resolved photoluminescence spectroscopy, which is the approach pursued in this work. In particular, we are focused on the possibility to incorporate angle tuning of the fluorescent light incident on the detection system, which offers a fast way of adjusting the phase matching in the non-linear optical mixing process. The detection system is operating in the wavelength range from 1.55 μm to 2.20 μm, and its characteristics are mapped out using scattered light from a pulsed laser. Finally, a comparison with a commercial PMT is done using a fluorescent sample emitting light around 1.55 μm.

The experimental setup is shown in Fig. 1. Starting in the lower-left corner of Fig. 1(a), a pump laser may excite a sample under investigation, and the emitted IR light is imaged (with a magnification factor of 2) via various flat and curved mirrors to a Princeton Instruments spectrograph, consisting of "Monochromator 1" (Acton SP2358) and a PyLoN-IR:1024-1.7 InGaAs photodiode detector array. This spectrograph is also equipped with a Hamamatsu R5509-73 PMT and represents a rather standard commercial setup for steady-state and time-resolved fluorescence detection for wavelengths up to 1.7 μm. Using a flip mirror, it is possible to divert the light towards the UCD system. The sample fluorescence is imaged (with an additional magnification factor of 3.4) onto a motorized mirror, the rotation of

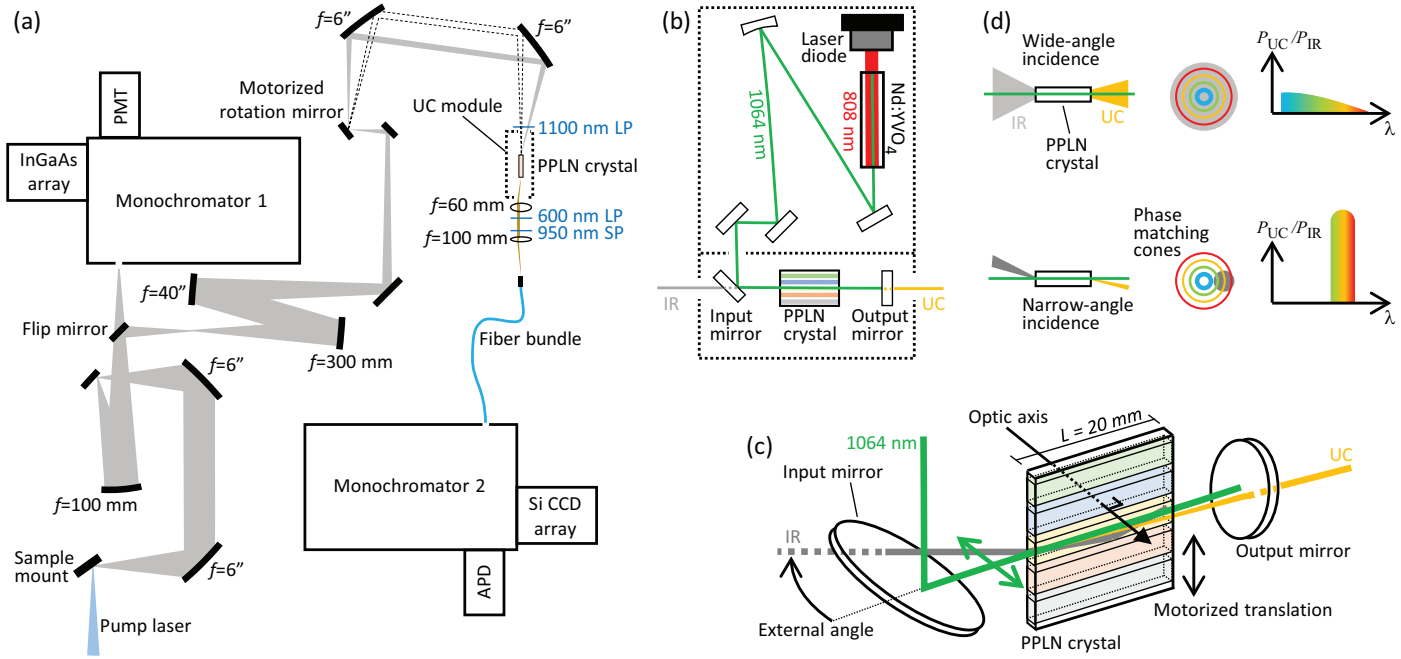


**Fig. 1.** (a) Top view of the optical beam path with IR photoluminescence shown in gray. Curved mirrors with $f = 6''$ are 90° off-axis parabolic mirrors, and SP and LP denote short- and long-pass filters, respectively. (b) Side view of the upconverter module. (c) Beam paths through the PPLN crystal with the five channels emphasized using different colors. (d) A comparative sketch of wide and narrow angular spectrum of the IR light incident on the PPLN crystal.

which controls the incidence angle of the fluorescence onto a periodically poled lithium niobate (PPLN) crystal via two curved mirrors. The PPLN crystal is kept at a constant temperature of 25 °C and enclosed in an upconverter module as depicted in Fig. 1(b), where the incoming IR fluorescence is mixed with a laser beam of wavelength $\lambda_L = 1064$ nm, originating from a diode-laser pumped Nd:$YVO_4$ crystal and with an intra-cavity power of typically $\sim 30$ W $\pm$ 10 % (may drift slowly over minutes). As detailed in Fig. 1(c), the PPLN crystal consists of five channels with poling periods $\Lambda = 11.8$, 12.8, 13.8, 14.8, and 15.8 µm, which can be selected using a motorized translation stage. The outgoing UC light is imaged to an optical fiber bundle and directed into another Princenton Instruments spectrograph, consisting of "Monochromator 2" (Acton SP2358) and a PIXIS:100BR CCD camera, being equipped with a Perkin Elmer single-photon counting APD module.

The collection semi-angle of the first curved mirror after the sample is 9.5°, which due to the total magnification of 6.8 leads to an angular spread (semi-angle) of 1.4° for the light incident on the PPLN crystal input facet. The incidence angle can be varied between 0 and 16°, but due to refraction into the lithium niobate crystal (refractive index 2.13), the internal angle of the IR light is adjustable between 0° and 7.5° with a semi-angle spread of 0.66°. The advantage of using a rather narrow semi-angle is illustrated in Fig. 1(d), where the angular overlap between the incident IR fluorescence (gray circle) and the different phase-matching angles for different wavelengths (colored concentric rings) is sketched, leading to either a low sensitivity in a broad spectral range for a wide angular spectrum (exemplified in Ref. [3]) or a higher sensitivity in a limited spectral range for a narrow angular spectrum of the IR signal.

In order to characterize the performance of the UCD, with emphasis on the angle-tuning capability, we insert a white piece

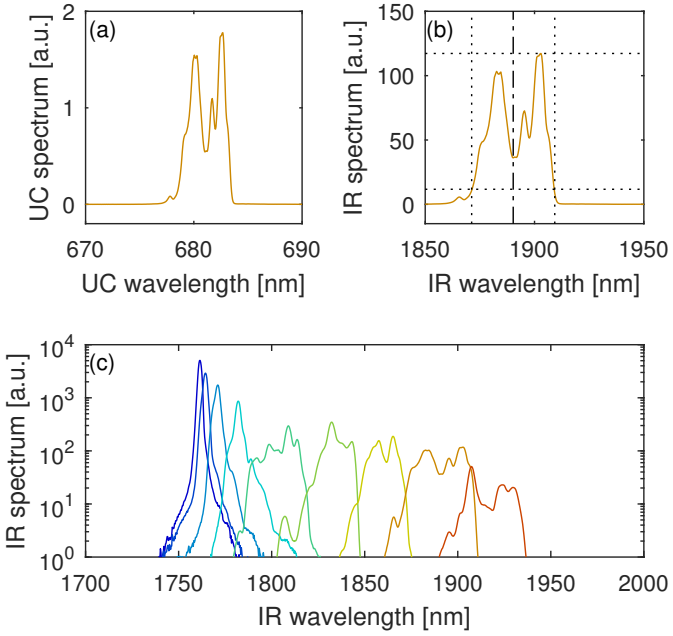


**Fig. 2.** (a) An example of a raw UC spectrum obtained with $\Lambda = 13.8$ µm and an incidence angle of 14° (internal angle 6.6°). (b) Apparent IR spectrum, normalized as described in the text. The horizontal dotted lines represent the maximum and 10-% value of the IR intensity. The separation between the vertical dotted lines defines the width of the spectrum, and the dash-dotted line represents the center wavelength of the spectrum. Panel (c) shows spectra corresponding to all investigated angles (from left, the incidence angle increases from 0 to 16°in steps of 2°).

of paper in the sample mount and illuminate this by an IR pulsed laser of tunable wavelength, obtained from a Spectra Physics TOPAS Prime parametric amplifier pumped by a Spectra Physics Solstice ACE femtosecond laser. A resulting measured spectrum of the UC light is exemplified in Fig. 2(a). Denoting the wavelengths of the IR and UC light by $\lambda_{\mathrm{IR}}$ and $\lambda_{\mathrm{UC}}$, respectively, the photon energy conservation of the mixing process requires that $\lambda_{\mathrm{UC}}^{-1} = \lambda_{\mathrm{L}}^{-1} + \lambda_{\mathrm{IR}}^{-1}$, and Fig. 2(a) hence shows a spectrum $S_{\mathrm{UC}}(\lambda_{\mathrm{UC}})$ at visible wavelengths. The *apparent* IR spectrum, $S_{\mathrm{IR}}(\lambda_{\mathrm{IR}})$, is then calculated as $S_{\mathrm{IR}}(\lambda_{\mathrm{IR}}) = S_{\mathrm{UC}}(\lambda_{\mathrm{UC}})\lambda_{\mathrm{UC}}^2/\lambda_{\mathrm{IR}}^2$, where $\lambda_{\mathrm{UC}}$ and $\lambda_{\mathrm{IR}}$ are related by the above-mentioned photon-energy-conservation equation, see Fig. 2(b). Note, that this is not the true IR spectrum of the scattered laser light reaching the PPLN crystal, since it is affected by the upconverter sensitivity and bandwidth. However, since the IR pulse is broad-band ($\sim$ 100 nm), and since we take care that the wavelength of the IR pulse stays very close to the center position of the apparent IR spectrum, $S_{\mathrm{IR}}(\lambda_{\mathrm{IR}})$, the properties of this spectrum, e.g. center position, width, and height, will characterize the upconversion process in terms of phase-matching wavelength, bandwidth, and sensitivity, respectively. The apparent spectrum has also been normalized to the IR pulse energy and to the intra-cavity power of the upconverter module. Fig. 2(c) exemplifies how the apparent spectra vary as a function of the incidence angle.

Referring to Fig. 2(b), the peak height is defined as the maximum value of the apparent IR spectrum, and the width corresponds to the region where the IR intensity is $\geq 10$ % of the peak height. The center wavelength is determined as the midpoint between the 10-%-intensity edges, and furthermore the peak area is calculated within these edges. All these characteristics are plotted in Fig. 3. The predicted wavelengths (dashed lines in Fig. 3(a)) have been calculated using the phase-matching condition, $\mathbf{k}_{\mathrm{UC}} = \mathbf{k}_{\mathrm{IR}} + \mathbf{k}_{\mathrm{L}} + \mathbf{k}_g$, where $\mathbf{k}_{\mathrm{UC}}$ and $\mathbf{k}_{\mathrm{IR}}$ represent the wave vector of the UC and IR light, respectively. $\mathbf{k}_{\mathrm{L}}$ and $\mathbf{k}_g$ correspond to the wave vector of the upconversion laser and the periodic poling, respectively, both being parallel to the PPLN channels. The magnitude of these vectors are $k_g = 2\pi/\Lambda$, and $k_i = 2\pi n(\lambda_i)/\lambda_i$ for $i =$ UC, IR, and L, where $n$ is the refractive index of the PPLN crystal. The small-angle approximation has been used along the lines of Ref. [8], in which case a weak angle dependence of the refractive index can be safely neglected, $n(\lambda, \theta) \approx n_{\mathrm{e}}(\lambda)$, with $n_{\mathrm{e}}$ being the refractive index for extraordinary polarization. Evidently, the agreement between observed center wavelengths and model predictions is good. The observed spectral widths, shown as the marker heights in Fig. 3(a), can largely be explained by the angular spread of the scattered light incident on the PPLN crystal, giving rise to simultaneous phase-matching at a range of wavelengths [3].

The areas and heights of the apparent IR spectra are plotted in Fig. 3(b) and Fig. 3(c), respectively. For the channel with $\Lambda = 11.8$ µm, the TOPAS is operating near its degeneracy point, preventing a thorough investigation of sensitivity and thus only leaving two data points. The variation in peak height can be explained primarily by geometrical variations in the interaction length, $L_{\mathrm{int}}$, between the IR and laser light within the PPLN crystal together with variations in the acceptance angle spread. The latter is defined by the range of angles, for which the phase mis-match fulfills $\Delta k \leq \pi/L_{\mathrm{int}}$. The internal IR acceptance angle spread is largest for collinear phase matching, ranging between 0.62° and 0.69° for the five PPLN channels and thus matching well with the semi-angle spread of the IR light. It is clearly possible to operate the UCD in a broad spectral range from 1.55 µm

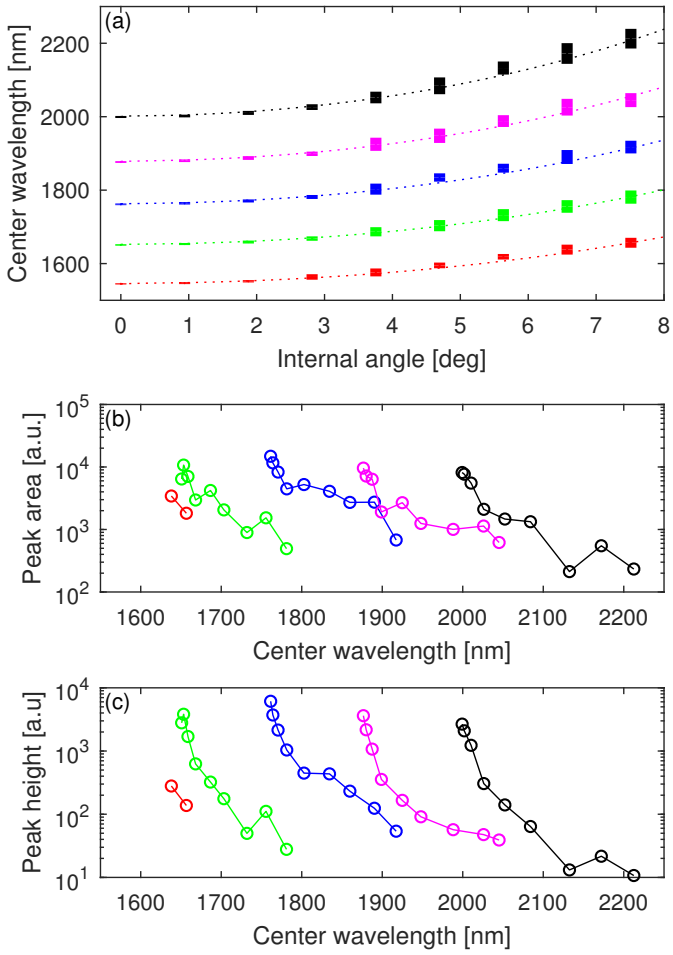


**Fig. 3.** (a) Center wavelength of the apparent IR spectrum as a function of the internal angle. The height of each rectangle corresponds to the spectral width. Each color corresponds to different channels in the PPLN crystal with poling periods (from below) 11.8 (red), 12.8 (green), 13.8 (blue), 14.8 (magenta), and 15.8 (black) µm. Dashed lines are theoretical predictions of the phase-matching wavelength. Panels (b) and (c) show the peak area and peak height, respectively, as a function of center wavelength with same color coding as in panel (a).

to 2.20 µm by simple mechanical adjustments within the optical system. Of course, this comes at the price that the non-collinear phase matching offers lower sensitivity. The apparent spectral peak area is typically reduced by an order of magnitude in the tuning range between the collinear phase-matching wavelengths corresponding to the used poling periods (see Fig. 3(b)), whereas the peak height is typically reduced by two orders of magnitude (Fig. 3(c)). The relevant figure of merit, peak area or peak height, depends on the specific wavelength resolution required in a specific application. An obvious alternative tuning method is changing the PPLN crystal temperature. Obtaining a continuous wavelength range with collinear phase matching would, for the poling periods used here, require the temperature to be adjusted between 0 °C and 300 °C, which would both be a slow process and result in stability issues for the intra-cavity laser field. One could imagine a combined tuning scheme, where an initial survey scan is undertaken by angle tuning, and later measurements with high signal-to-noise ratio at a few specific wavelengths could be performed using adjustments of the temperature.

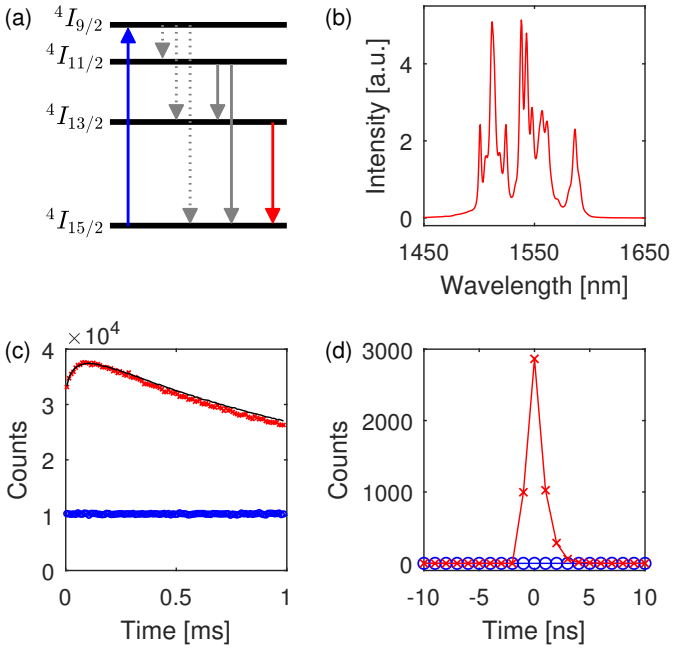


**Fig. 4.** (a) Relevant level diagram for $Er^{3+}$ ions embedded in $Gd_2O_2S$. The blue arrow corresponds to the pump laser at 800 nm wavelength, the red arrow to the observed luminescence near 1.55 µm, and the gray arrows denote non-observed transitions. (b) The spectrum of the $^4I_{13/2} \rightarrow {}^4I_{15/2}$-transition in $Er^{3+}$ obtained by an InGaAs detector array. (c) Decay curves of the $^4I_{13/2} \rightarrow {}^4I_{15/2}$-transition in $Er^{3+}$ measured by the UCD (red) and the background level with blocked pump laser (blue). Time bins are 10 µs wide. The black curve is obtained by the PMT and rescaled vertically to match the red decay curve. (d) Measured upconversion signal using the scattering from the pulsed laser at 1.55 µm as the IR signal source (red crosses). Blue circles correspond to a blocking of the pulsed laser.

In order to compare the performance of the UCD to the commercial PMT detector, a sample containing a film of Er- and Yb-doped $Gd_2O_2S$ nanoparticles is inserted into the sample mount and illuminated by a pulsed femto-second laser operating at a wavelength near 800 nm. Due to the erbium content of these nanoparticles, the sample will emit light near 1.55 µm, see the level structure in Fig. 4(a) and an experimentally obtained spectrum using the InGaAs detector array in Fig. 4(b). Decay curves obtained with the UCD and the PMT, are shown in Fig. 4(c). The UCD data was obtained with $\Lambda = 11.8$ µm and an internal angle of 0.4°. The vertical scale shows the actual counts measured by the APD after the upconverter module using an integration time of 15 minutes (i.e. $9 \cdot 10^5$ pulses). Upconverted parametric fluorescence noise from the PPLN crystal and dark counts from the APD contribute in total $1.1 \cdot 10^3$ counts/s to the blue curve, and additional $2.4 \cdot 10^3$ count/s originate as signal counts from the erbium fluorescence to form the red curve. The effective detector area of the PPLN crystal, set by the $1/e^2$ beam radius $w = 180$ µm of the Nd:$YVO_4$ laser beam, is $\pi w^2 = 1.0 \cdot 10^5$ µm$^2$, corresponding to an imaged area on the sample of $2.2 \cdot 10^3$ µm$^2$ (taking the magnification into account). The diameter of the pulsed laser on the sample is $\sim 0.5$ mm, and by adjusting the entrance slit of "Monochromator 1" to 10 µm, the imaged area, using the PMT and taking the magnification into account, is then $2.5 \cdot 10^3$ µm$^2$, i.e. similar to the UCD. The spectral resolution of the PMT detection is estimated to be an order of magnitude narrower than that of the UCD, and in contrast to the PMT, the UCD is only sensitive to one polarization direction parallel to the optic axis of the PPLN crystal. Acquiring a decay curve using the PMT for 1.5 min., with and without the pulsed laser on, generates a decay curve of similar shape as was obtained for the UCD, see Fig. 4(c), with a total dark count rate of $8.8 \cdot 10^4$ counts/s and with additional $3.3 \cdot 10^5$ signal counts/s. While count rates with the PMT are approximately two orders of magnitude larger than those for the UCD, the ratio of signal to dark counts remains roughly the same. The count rate of the UCD could be further optimized by replacing the APD with another detector with larger active area and/or removing the fiber bundle to minimize coupling loss. The example luminescence decay measurement is only at 1.55 µm, where the PMT has its maximum sensitivity. The sensitivity of the PMT is reduced by two orders of magnitude or more at longer wavelengths (1.7 µm $< \lambda_{IR} <$ 2.2 µm), where the UCD has greater potential.

Finally, to demonstrate the timing resolution of the UCD, the pulsed laser is tuned to 1.55 µm and scattered on a piece of paper in the sample mount. The UC light is detected by the APD after "Monochromator 2", leading to the instrument response function of Fig. 4(d), which, with its FWHM duration of $\sim 2$ ns, allows for ns-resolution time-resolved spectroscopy. This FWHM duration is limited by the timing jitter of the APD.

The detection scheme can easily be extended to longer wavelengths (up to 5 µm) by choosing a longer PPLN poling period $\Lambda$. Interesting physical systems to be studied could be, for instance, bulk [9] or nanocrystalline [10] GeSn alloys, where luminescence decay curves and corresponding lifetimes at selected wavelengths could provide important information about, among others, the direct/indirect nature of the radiative recombination [11] and about the dynamical behavior of laser materials [12].

**Funding:** This work was supported by the Villum Foundation and the Mid-TECH – H2020-MSCA-ITN-2014 (642661).

## REFERENCES

1. J. R. Lakowicz, *Principles of fluorescence spectroscopy* (Springer, New York, 2006), 3rd ed.
2. J. Shah, IEEE J. Quant. Elec. **24**, 276 (1988).
3. L. M. Kehlet, P. Tidemand-Lichtenberg, J. S. Dam, and C. Pedersen, Opt. Lett. **40**, 938 (2015).
4. L. Meng, A. Fix, M. Wirth, L. Høgstedt, P. Tidemand-Lichtenberg, C. Pedersen, and P. J. Rodrigo, Opt. Express **26**, 3850 (2018).
5. J. S. Dam, P. Tidemand-Lichtenberg, and C. Pedersen, Nat. Photon. **6**, 788 (2012).
6. A. Korneev, V. Matvienko, O. Minaeva, I. Milostnaya, I. Rubtsova, G. Chulkova, K. Smirnov, V. Voronov, G. Gol'tsman, W. Słysz, A. Pearlman, A. Verevkin, and R. Sobolewski, IEEE Trans. Appl. Supercond. **15**, 571 (2005).
7. A. Dumas, J. Rothman, F. Gibert, D. Édouart, G. Lasfargues, C. Cénac, F. L. Mounier, J. Pellegrino, J. Zanatta, A. Bardoux, F. Tinto, and P. Flamant, Appl. Opt. **56**, 7577 (2017).
8. H. Maestre, A. J. Torregrosa, and J. Capmany, Opt. Express **24**, 8581 (2016).
9. S. Wirths, R. Geiger, N. von den Driesch, G. Mussler, T. Stoica, S. Mantl, Z. Ikonic, M. Luysberg, S. Chiussi, J. M. Hartmann, H. Sigg, J. Faist, D. Buca, and D. Grützmacher, Nat. Photon. **9**, 88 (2015).
10. K. Ramasamy, P. G. Kotula, A. F. Fidler, M. T. Brumbach, J. M. Pietryga, and S. A. Ivanov, Chem. Mater. **27**, 4640 (2015).
11. D. Stange, S. Wirths, N. von den Driesch, G. Mussler, T. Stoica, Z. Ikonic, J. M. Hartmann, S. Mantl, D. Grützmacher, and D. Buca, ACS Photon. **2**, 1539 (2015).
12. L. Khriachtchev, M. Räsänen, S. Novikov, and J. Sinkkonen, Appl. Phys. Lett. **79**, 1249 (2001).

## FULL REFERENCES


1. J. R. Lakowicz, *Principles of fluorescence spectroscopy* (Springer, New York, 2006), 3rd ed.
2. J. Shah, "Ultrafast luminescence spectroscopy using sum frequency generation," IEEE J. Quant. Elec. **24**, 276 (1988).
3. L. M. Kehlet, P. Tidemand-Lichtenberg, J. S. Dam, and C. Pedersen, "Infrared upconversion hyperspectral imaging," Opt. Lett. **40**, 938 (2015).
4. L. Meng, A. Fix, M. Wirth, L. Høgstedt, P. Tidemand-Lichtenberg, C. Pedersen, and P. J. Rodrigo, "Upconversion detector for range-resolved dial measurement of atmospheric $ch_4$," Opt. Express **26**, 3850 (2018).
5. J. S. Dam, P. Tidemand-Lichtenberg, and C. Pedersen, "Room-temperature mid-infrared single-photon spectral imaging," Nat. Photon. **6**, 788 (2012).
6. A. Korneev, V. Matvienko, O. Minaeva, I. Milostnaya, I. Rubtsova, G. Chulkova, K. Smirnov, V. Voronov, G. Gol'tsman, W. Słysz, A. Pearlman, A. Verevkin, and R. Sobolewski, "Quantum efficiency and noise equivalent power of nanostructured, nbn, single-photon detectors in the wavelength range from visible to infrared," IEEE Trans. Appl. Supercond. **15**, 571 (2005).
7. A. Dumas, J. Rothman, F. Gibert, D. Édouart, G. Lasfargues, C. Cénac, F. L. Mounier, J. Pellegrino, J. Zanatta, A. Bardoux, F. Tinto, and P. Flamant, "Evaluation of a hgcdte e-apd based detector for 2$\mu$m $co_2$ dial application," Appl. Opt. **56**, 7577 (2017).
8. H. Maestre, A. J. Torregrosa, and J. Capmany, "Ir image upconversion using band-limited ase illumination fiber sources," Opt. Express **24**, 8581 (2016).
9. S. Wirths, R. Geiger, N. von den Driesch, G. Mussler, T. Stoica, S. Mantl, Z. Ikonic, M. Luysberg, S. Chiussi, J. M. Hartmann, H. Sigg, J. Faist, D. Buca, and D. Grützmacher, "Lasing in direct-bandgap gesn alloy grown on si," Nat. Photon. **9**, 88 (2015).
10. K. Ramasamy, P. G. Kotula, A. F. Fidler, M. T. Brumbach, J. M. Pietryga, and S. A. Ivanov, "$Sn_xge_{1-x}$ alloy nanocrystals: A first step toward solution-processed group iv photovoltaics," Chem. Mater. **27**, 4640 (2015).
11. D. Stange, S. Wirths, N. von den Driesch, G. Mussler, T. Stoica, Z. Ikonic, J. M. Hartmann, S. Mantl, D. Grützmacher, and D. Buca, "Optical transitions in direct-bandgap $ge_{1-x}sn_x$ alloys," ACS Photon. **2**, 1539 (2015).
12. L. Khriachtchev, M. Räsänen, S. Novikov, and J. Sinkkonen, "Optical gain in si/$sio_2$ lattice: Experimental evidence with nanosecond pulses," Appl. Phys. Lett. **79**, 1249 (2001).